

Multiple Coulomb excitation of the transitional nucleus ^{82}Kr

S. Brüssermann

II. Physikalisches Institut, Universität Göttingen, D-3400 Göttingen, Federal Republic of Germany

K. P. Lieb and P. Sona

*II. Physikalisches Institut, Universität Göttingen, D-3400 Göttingen, Federal Republic of Germany
and Dipartimento di Fisica, Università di Firenze, I-50125 Firenze, Italy*

H. Emling and E. Grosse

Gesellschaft für Schwerionenforschung, D-6100 Darmstadt, Federal Republic of Germany

J. Stachel*

Institut für Kernchemie, Universität Mainz, D-6500 Mainz, Federal Republic of Germany

(Received 20 May 1985)

A 4.6 MeV/nucleon ^{82}Kr beam has been used to Coulomb excite ^{82}Kr in collisions with a thin ^{208}Pb target. The backscattered projectiles were measured in a position sensitive avalanche detector centered around the beam axis. The gamma radiation was measured in four Ge(Li) detectors, in coincidence with the particles. The gamma ray spectra, after event-by-event Doppler shift correction, revealed 16 transitions in ^{82}Kr from the relative intensities of which a total of 22 electric quadrupole transition matrix elements have been deduced, by inserting the previously measured branching and mixing ratios. The level energies and $E2$ transition probabilities have been compared with the predictions of the asymmetric rotor, interacting boson, and Gneuss-Greiner models and nuclear field theory. On the basis of its energy and decay modes, the 1957 keV 2_3^+ state is interpreted as the lowest state with lower F spin, $F = F_{\text{max}} - 1 = 2$.

I. INTRODUCTION

Considerable experimental and theoretical effort has been devoted in recent years to clarify the structure of the even krypton isotopes.¹⁻⁸ In particular for ^{82}Kr two recent studies of the β decays of ^{82}Rb and ^{82}Br (Ref. 6) and the $^{80}\text{Se}(\alpha,2n)$ reaction⁷ have established the decay scheme of states up to about 6 MeV excitation energy. In addition to the ground band, several bands based on aligned two-quasiparticle excitations have been identified at moderate spin,^{7,8} leading to a pronounced backbending in the ground band at $I^\pi = 8^+$. The results have been interpreted in the frame of the cranked shell model,⁷ the interacting boson (IBA-2) model,^{6,9} the approach of the nuclear field theory,¹⁰ and in terms of the model of Gneuss and Greiner.¹¹ An interesting question emerging from these studies is whether the two-quasiparticle excitations can already influence the properties of the collective bands for low spin values, so as to make doubtful a consistent application of collective models, at least in their standard forms. An answer to this question could be provided by a detailed study of the transition rates between low spin members of the bands. Indeed several transition rates in ^{82}Kr have been already measured by Brüssermann *et al.*⁸ and by Kemnitz *et al.*⁷ by the recoil distance and the Doppler shift attenuation method. These authors employed the $^{76}\text{Ge}(^{12}\text{C},\alpha 2n)$ and $^{80}\text{Se}(\alpha,2n)$ reactions, respectively, to populate the final nucleus. However, the accuracy of the lifetime measurements for the low spin states has been severely limited by the presence of long lived

states which feed the lower ones. In particular, the long lifetimes of the 3462 keV 8_1^+ and 3038 keV 6_1^- states which collect large fractions of the gamma ray flux in the heavy ion induced compound reaction have so far prevented the determination of the lifetimes of the lowest states of the ground and the gamma bands in ^{82}Kr .

For stable nuclei multiple Coulomb excitation (MCE) offers an important alternative for determining $E2$ transition rates between low lying levels. In favorable cases^{12,13} MCE can also provide information on static quadrupole moments of higher yrast states as demonstrated recently by Stachel *et al.*¹² for the transitional nucleus ^{104}Ru . The aim of the present work was to use this method to determine transitional and static $E2$ moments in ^{82}Kr so as to make possible a meaningful comparison with the predictions of different models.

II. EXPERIMENT

A 3 particle nA beam of ^{82}Kr ions at 4.6 MeV/nucleon produced at the UNILAC accelerator at Gesellschaft für Schwerionenforschung (GSI) was used to bombard a 400 $\mu\text{g}/\text{cm}^2$ ^{208}Pb target. The ^{82}Kr ions backscattered from the target were detected in a position-sensitive avalanche counter (PPAC) which is schematically shown in Fig. 1. The counter was similar to the one described by Stelzer¹⁴ and Gaukler *et al.*¹⁵ and was built in collaboration with the detector laboratory at GSI.

The counter had axial symmetry and was centered in the axis of the beam which reached the target through a

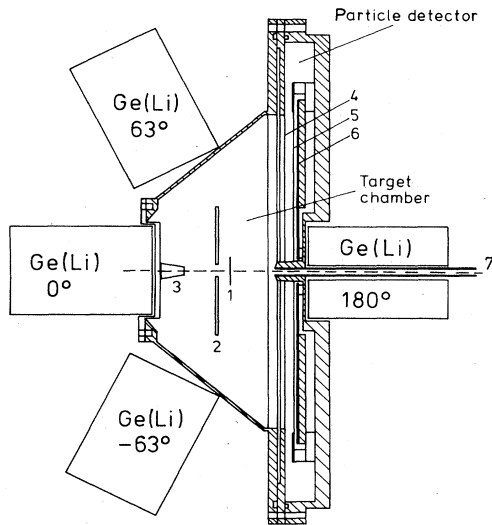


FIG. 1. Schematic view of the experimental setup: (1) thin ^{208}Pb target, (2) Al frame, (3) beam stop, (4) entrance foil, (5) anode, (6) cathode of avalanche detector, (7) beam.

hole in the center. In this way, the counter covered the full azimuthal range $0^\circ \leq \Phi \leq 360^\circ$. The distance from the target was such as to cover polar angles θ in the range $110^\circ \leq \theta \leq 167^\circ$; these limits correspond to a solid angle of 3.8 sr in the center of mass system. The position sensitivity in θ and Φ was achieved as follows: The cathode consisted of a pattern of 50 concentric rings etched on a printed circuit board. Each ring was 2.5 mm wide and was separated from its neighbor by a 0.5 mm gap. The cathode signal was read out by means of a LC delay line giving a 3 ns delay between neighboring rings. In this way the polar angle of backscattered Kr ions was directly determined by the delay of the cathode pulse with respect to the anode signal, which gave the prompt signal. The

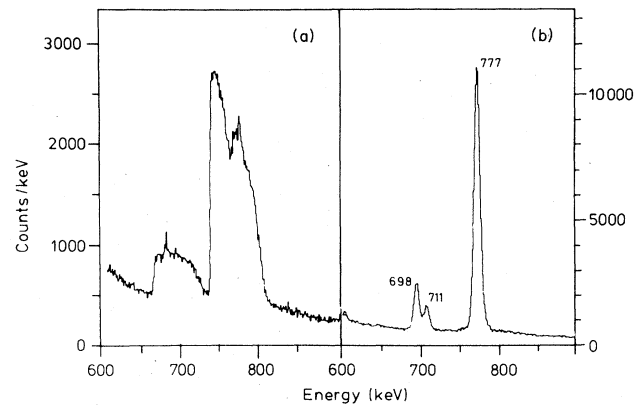


FIG. 2. Effect of the Doppler correction on the gamma ray lines in the 600–900 keV region: (a) raw spectrum; (b) Doppler corrected spectrum.

anode consisted of a Mylar foil (30 cm in diameter, 1.5 μm thick) metalized on one side by a $50 \mu\text{g}/\text{cm}^2$ silver layer deposited by vacuum evaporation. It was mounted at a distance of 2.5 mm from the cathode and was divided in 20 sectors each covering an azimuthal range of 18° . The prompt signal of each segment was read out independently to obtain the azimuth of the scattered ions. A voltage of +600 V was applied to each sector through 1 M Ω resistors. A second 1.5 μm Mylar foil served to separate the detector volume, filled with 13 mbar isobutane, from the scattering chamber. The foil was backed by a highly transparent grid of 0.1 mm wires. The gas in the counter which had a sensitive volume of $\approx 1300 \text{ cm}^3$ was continuously refreshed at a rate of $\approx 2 \text{ cm}^3/\text{s}$.

After passing the target, the beam was stopped in a 1 mm thick foil of natural lead. A 0.1 mm thick aluminum diaphragm was placed 1.2 cm downstream of the target and prevented Kr ions backscattered at the beam stopper

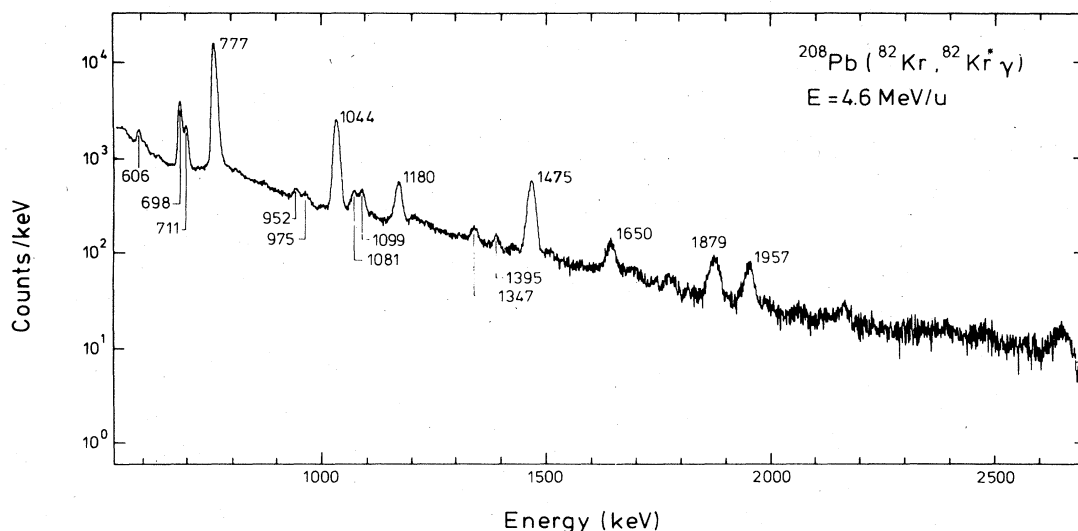


FIG. 3. Total Doppler corrected spectrum summed over all Ge detectors and particle angles.

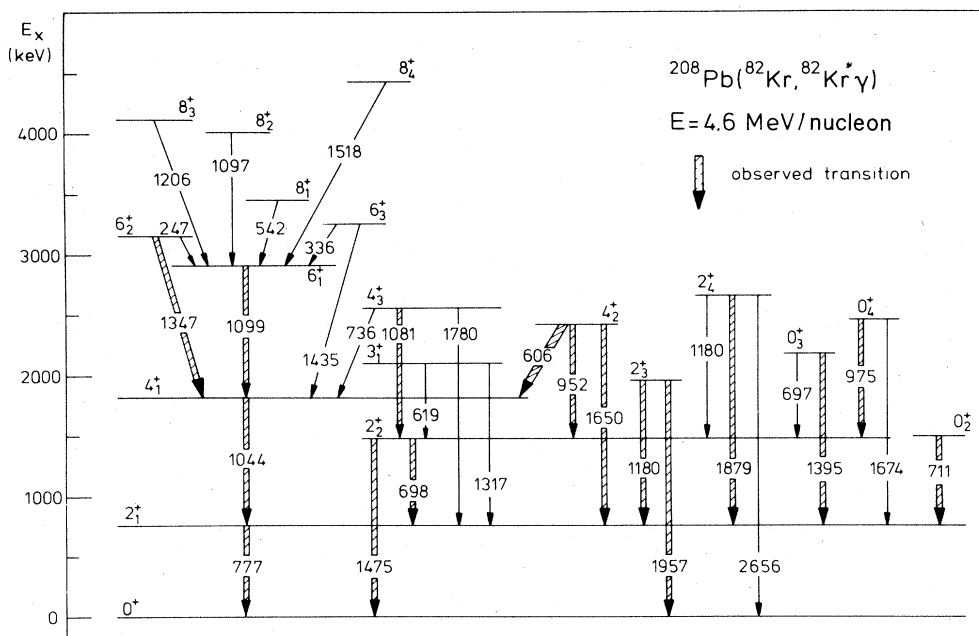


FIG. 4. Level scheme (Refs. 6 and 7) used in the calculation of the Coulomb excitation cross sections $\sigma_I(\theta)$. The observed transitions are marked.

from reaching the PPAC. In addition, a 20 mm thick conical tungsten shield was placed just behind the beam stopper to avoid excessive loading of the 0° germanium detector by x rays generated in the beam stop (see Fig. 1).

Gamma rays were recorded by four Ge detectors each having about 30% photopeak efficiency relative to a 7.5 cm \times 7.5 cm NaI crystal. They were positioned at $\pm 63^\circ$, 0° , and 180° to the beam direction. The detectors at $\pm 63^\circ$ were located with the front ends of their crystals at a distance 11 cm from the target, thus each covering a solid angle of 140 msr; the 0° and 180° detectors were at a distance of 7 cm from the target and covered a solid angle of 240 msr.

All germanium detectors were operated in coincidence with backscattered ^{82}Kr projectiles. The data were collected event by event and stored on magnetic tape for subsequent off-line analysis. Each event consisted of the (θ, Φ) position and the time information of the particle and the time and energy information of each germanium detector.

Because of the high recoil velocities of the ions after scattering ($0.041 \leq v/c \leq 0.054$) a large Doppler shift and broadening was observed in the gamma ray spectra [see (a) of Fig. 2]. The spectra were corrected event by event by calculating the Doppler shift to second order of v/c for a gamma ray recorded at the angle θ_γ in coincidence with a ^{82}Kr ion detected at angles (θ, Φ) . In making this correction the scattering process was assumed to be elastic. The spectrum obtained after correction is shown in Fig. 2(b), while the Doppler corrected full spectrum, summed over all particle angles and γ -ray detectors, is displayed in Fig. 3. The resulting energy resolution was 10 keV (FWHM)

TABLE I. Experimental gamma ray yield ratios $R_{f \rightarrow r}^f(\theta, \theta_\gamma)$.

| E_γ (keV) | Gamma ray yield ratio ^a (10^3) | | | |
|----------------------------|---|----------------------|----------------------|----------------------|
| | $\theta = 164^\circ$ | $\theta = 152^\circ$ | $\theta = 144^\circ$ | $\theta = 136^\circ$ |
| $\theta_\gamma = 0^\circ$ | | | | |
| 606 | 34.3(59) | 36.5(59) | 41.9(70) | 51.4(83) |
| 698 | 224(33) | 209(33) | 201(32) | 202(32) |
| 711 | 96(12) | 87(14) | 64(12) | 52(9) |
| 1044 | 267(30) | 276(31) | 277(31) | 296(32) |
| 1081 | 21.2(39) | 27.9(47) | 25.6(45) | 26.3(52) |
| 1099 | 24.0(43) | 29.1(58) | 31.0(59) | 39.8(65) |
| 1180 | 70(12) | 54(9) | 47(8) | 43(6) |
| 1475 | 93(17) | 85(10) | 85(12) | 91(10) |
| 1650 | 23.5(46) | 25.4(48) | 17.8(30) | 19.5(33) |
| 1879 | 27.8(42) | 15.4(25) | 13.6(24) | 16.0(34) |
| 1957 | 17.7(67) | 8.6(20) | 10.1(22) | 8.3(18) |
| $\theta_\gamma = 63^\circ$ | | | | |
| 606 | 24.6(77) | 24.0(48) | 21.1(37) | 21.9(38) |
| 698 | 164(26) | 153(24) | 150(23) | 138(24) |
| 711 | 88(10) | 79(9) | 73(12) | 58(11) |
| 1044 | 196(22) | 214(23) | 230(25) | 232(25) |
| 1081 | 22.2(29) | 17.8(32) | 19.8(36) | 18.6(38) |
| 1099 | 21.1(28) | 23.5(39) | 22.9(40) | 26.6(46) |
| 1180 | 59(8) | 52(8) | 48(8) | 42(7) |
| 1475 | 116(19) | 103(17) | 100(15) | 83(10) |
| 1650 | 21.8(33) | 16.3(27) | 17.5(25) | 14.2(37) |
| 1879 | 24.3(44) | 22.7(30) | 14.8(22) | 13.2(24) |
| 1957 | 24.9(45) | 20.4(35) | 17.2(29) | 18.0(23) |

^aNormalized with respect to the intensity of the 777 keV transition.

TABLE II. Measured and fitted integral gamma ray yield ratios at $\theta_\gamma=0^\circ$ and 63° , normalized with respect to the integral yield of the 777 keV transition.

| E_γ (keV) | $\theta_\gamma=0^\circ$ | | $\theta_\gamma=63^\circ$ | |
|---------------------|---|---|---|---|
| | $R_{I \rightarrow I'}^f(\theta_\gamma)^a$ | $R_{I \rightarrow I'}^i(\theta_\gamma)^a$ | $R_{I \rightarrow I'}^f(\theta_\gamma)^a$ | $R_{I \rightarrow I'}^i(\theta_\gamma)^a$ |
| 606 | 37.8(61) | 23.5 | 21.3(37) | 24.2 |
| 698 | 202(33) | 176 | 150(24) | 162 |
| 711 | 75(12) | 69 | 74(12) | 72 |
| 952 | 14.0(24) | 6.0 | 8.5(16) | 5.0 |
| 975 | 16.2(34) | 4.4 | 4.7(12) | 4.6 |
| 1044 | 280(33) | 264 | 217(25) | 219 |
| 1081 | 26.1(43) | 24.1 | 18.9(34) | 19.9 |
| 1099 | 30.0(50) | 29.2 | 21.9(36) | 24.2 |
| 1180 | 51(8) | 57 | 49(8) | 43 |
| 1347 | 8.7(15) | 10.5 | 8.4(16) | 8.6 |
| 1395 | 4.2(9) | 4.2 | 4.6(10) | 4.4 |
| 1475 | 88(10) | 91 | 99(13) | 87 |
| 1650 | 20.2(26) | 21.0 | 16.0(20) | 17.0 |
| 1879 | 16.0(23) | 17.9 | 17.3(21) | 14.9 |
| 1957 | 8.7(14) | 11.6 | 20.0(32) | 14.8 |

^aIn units of 10^3 of yield of 777 keV transition.

at 777 keV ($2_1^+ \rightarrow 0_1^+$ transition) and 17 keV at 2000 keV. The main contribution to the energy resolution was due to the finite angular resolution of the PPAC.

All observed gamma rays could be attributed to ^{82}Kr according to the known level scheme,^{6,7} states up to 3167 keV and $I=6$ were observed (see Figs. 3 and 4). Table I lists the measured intensity ratios of the observed transitions relative to the 777 keV $2_1^+ \rightarrow 0_1^+$ transition:

$$R_{I \rightarrow I'}^f(\theta, \theta_\gamma) = \frac{Y_{I \rightarrow I'}(\theta, \theta_\gamma)}{Y_{2 \rightarrow 0}(\theta, \theta_\gamma)}. \quad (1)$$

In order to accumulate more statistics we summed the gamma ray yields within the following four polar windows: $157.5^\circ \leq \theta \leq 172.5^\circ$, $147.1^\circ \leq \theta \leq 157.5^\circ$, $140.6^\circ \leq \theta \leq 147.1^\circ$, and $132.2^\circ \leq \theta \leq 140.6^\circ$. For all transitions the yield was also integrated over the full θ range covered by the particle detector; these "integral" values are summarized in Table II. The uncertainties given include the statistical errors, those from the unfolding procedure, and a 10% systematic error which is mostly due to the response of the particle detector.

III. DETERMINATION OF THE $E2$ MATRIX ELEMENTS

A. Safe energy

The dominant process in MCE is the excitation of nuclear states connected by large $E2$ transitional moments. If the nuclear force plays no role during the collision, it is possible to calculate with high accuracy the excitation cross section for each level starting from a given set of transitional and static electromagnetic moments. The conditions for neglecting the influence of the nuclear interaction are satisfied in our experiment. In fact, at a bombarding energy of 4.6 MeV/nucleon for ^{82}Kr nuclei on ^{208}Pb , the distance of closest approach ($a = 15.7$ fm at

$\theta = 172.5^\circ$) exceeds the sum of the radii of the colliding nuclei, $R_1 + R_2 = 12.3$ fm ($r_0 = 1.2$ fm), by 3.4 fm. Under such conditions it has been estimated that the excitation cross sections are not affected by more than 3%.^{12,15}

B. Outline of the fitting procedure

The method used to determine the matrix elements consists essentially of a linearized iterative χ^2 minimization procedure whereby the experimental yields for deexciting gamma rays are compared with those calculated by means of a MCE computer code. A set of "starting values" for the reduced $E2$ matrix elements $\mathcal{M}_k = \langle I_{fk} || M(E2) || I_{ik} \rangle$ are required as input data for the code. At each iteration step "corrections" $\{\delta \mathcal{M}_k\}$ are obtained as the solution of linearized equations (see below) and the new set of matrix elements $\{\mathcal{M}_k + \delta \mathcal{M}_k\}$ is used as input for the next iteration until convergence is reached.

Before performing the calculations, one has first to decide, on the basis of the observed gamma rays and decay scheme, which levels are likely to be excited and significantly affect the gamma ray yields, trying at the same time to keep their number at a minimum in order to save computing time. The level scheme considered in our calculations is based mostly on the work of Meyer *et al.*⁶ and Kemnitz *et al.*⁷ and is shown in Fig. 4.

To further limit the number of free parameters, i.e., the numbers of independent matrix elements to be determined, we also used available experimental data on gamma ray branching ratios, $E2/M1$ mixing ratios, and matrix elements known from previous experiments. These known parameters are summarized in Table III. All gamma ray yields have been normalized with respect to the 777 keV $2_1^+ \rightarrow 0_1^+$ transition (see Fig. 3). The $B(E2)$ value of this transition $B(E2, 2_1^+ \rightarrow 0_1^+) = 450(21) e^2 \text{fm}^4$ has been obtained with good accuracy by Keinonen *et al.*⁵ in a Coulomb excitation experiment of 1.4 MeV/nucleon ^{82}Kr ions on thick ^{27}Al and Ge targets.

TABLE III. $E2$ matrix elements \mathcal{M} , branching ratios, and $E2/M1$ mixing ratios (Refs. 5–8) used as input parameters in the fit of the γ -ray intensities.

| E_γ (keV) | I_i^π | I_f^π | \mathcal{M} (e b) | Branching ratio (%) | Mixing ratio e b/ μ_n | Ref. |
|---------------------|-----------|-----------|------------------------|---------------------------|---------------------------------|--------|
| 1518 | 8_4^+ | 6_1^+ | 0.80(20) | 93(3) | | 7 |
| 1206 | 8_3^+ | 6_1^+ | 0.15(4) | 32(2) | | 7 |
| 1097 | 8_2^+ | 6_1^+ | 0.64(7) | 74(4) | | 7 |
| 542 | 8_1^+ | 6_1^+ | 0.465(44) | 100 | | 7,8 |
| 1435 | 6_3^+ | 4_1^+ | 0.51(11) | 78(3) | | 7 |
| 1347 | 6_2^+ | 4_1^+ | | 91(2) | | 6,7 |
| 1099 | 6_1^+ | 4_1^+ | | 100 | | |
| 1181 | 2_4^+ | 2_2^+ | | 18(7) | | 6 |
| 1879 | | 2_1^+ | | 59(6) | $\approx 1.85^a$ | |
| 2656 | | 0_1^+ | | 15(3) | | |
| 1168 | | 0_2^+ | | 8(3) | | |
| 736 | 4_3^+ | 4_1^+ | | 8(1) | | 6,7 |
| 1081 | | 2_2^+ | | 72(1) | | |
| 1779 | | 2_1^+ | | 14(1) | | |
| 975 | 0_4^+ | 2_2^+ | | 54(4) | | 6 |
| 1674 | | 2_1^+ | | 46(4) | | |
| 606 | 4_2^+ | 4_1^+ | | 50(9) | $-0.41(5)$ | 6,22 |
| 952 | | 2_2^+ | | 15(5) | | |
| 1650 | | 2_1^+ | | 32(5) | | |
| 697 | 0_3^+ | 2_2^+ | | 12.7(4) | | 6 |
| 1395 | | 2_1^+ | | 87.3(4) | | |
| 1180 | 2_3^+ | 2_1^+ | | 70(1) | $\approx 1.4^a$ | 6 |
| 1957 | | 0_1^+ | | 30(1) | | |
| 1044 | 4_1^+ | 2_1^+ | | 100 | | |
| 711 | 0_2^+ | 2_1^+ | | 100 | | 6 |
| 698 | 2_2^+ | 2_1^+ | | 63.0(4) | 2.5(3) | 6,7,22 |
| 1475 | | 0_1^+ | | 37.0(4) | | |
| 777 | 2_1^+ | 0_1^+ | 0.474(10) | 100 | | 5 |

^aDeduced in this experiment.

To perform the calculations we used a modified version of the de Boer-Winter program.¹⁶ This program uses the semiclassical approximation to calculate the excitation cross section $\sigma_I(\theta)$ for each state I as a function of the c.m. scattering angle θ . The approximation is well justified in our case since the Sommerfeld parameter ($\eta \approx 216$) is much larger than the maximum spin considered ($I_{\max} = 8$). The polarization correction due to the virtual excitation of the giant resonance has been included in the calculations according to the estimate given in the monograph of Alder and Winther.¹⁶ As a result of this part of the calculation one obtains the excitation cross section $\sigma_I(\theta)$ for each level I as well as its alignment described by a set of statistical tensors. The program then computes for each transition $I \rightarrow I'$ the yield $Y_{I \rightarrow I'}(\theta, \theta_\gamma)$. At this stage the program takes into account the different decay paths which, by gamma or internal conversion electron emission, lead from the excited state I to the state I' , the effect of unobserved transitions in between, and the deorientation effects.

C. Deorientation effects

Hyperfine deorientation of highly charged ions recoiling into vacuum can significantly alter the particle-

gamma correlation pattern, especially for long lived states.^{12,13,17} At velocities of the order of a percent of the velocity of light, the deorientation of the nuclear spin, observed in a time integrated measurement, is rather well described by the Abragam-Pound model.¹⁸ In this model the time integrated attenuation coefficients are given by

$$G_k = 1/(1 + \lambda_k \tau), \quad k = 0, 2, 4. \quad (2)$$

The parameter λ_k is proportional to the magnetic hyperfine field, the g factor of the nuclear level, and the correlation time τ_c . To get the value of λ_k we fitted the theoretical double ratio

$$G_{I \rightarrow I'}(\theta) = \frac{R_{I \rightarrow I'}^i(\theta, \theta_\gamma = 0^\circ, \{\mathcal{M}_k\})}{R_{I \rightarrow I'}^f(\theta, \theta_\gamma = 63^\circ, \{\mathcal{M}_k\})} \quad (3)$$

to the corresponding experimental ratio. This experimental ratio is independent of the different absolute efficiencies of the Ge(Li) detectors, but depends sensitively on the γ -ray angular correlation.

We now choose short lived nuclear states in ^{82}Kr ($\tau \leq 2.1$ ps) decaying by pure $E2$ transitions to first get the attenuation coefficient of the $2_1^+ \rightarrow 0_1^+$ normalizing transition. Assuming that the g factors of all nuclear levels excited in this experiment are the same as that of the 2_1^+

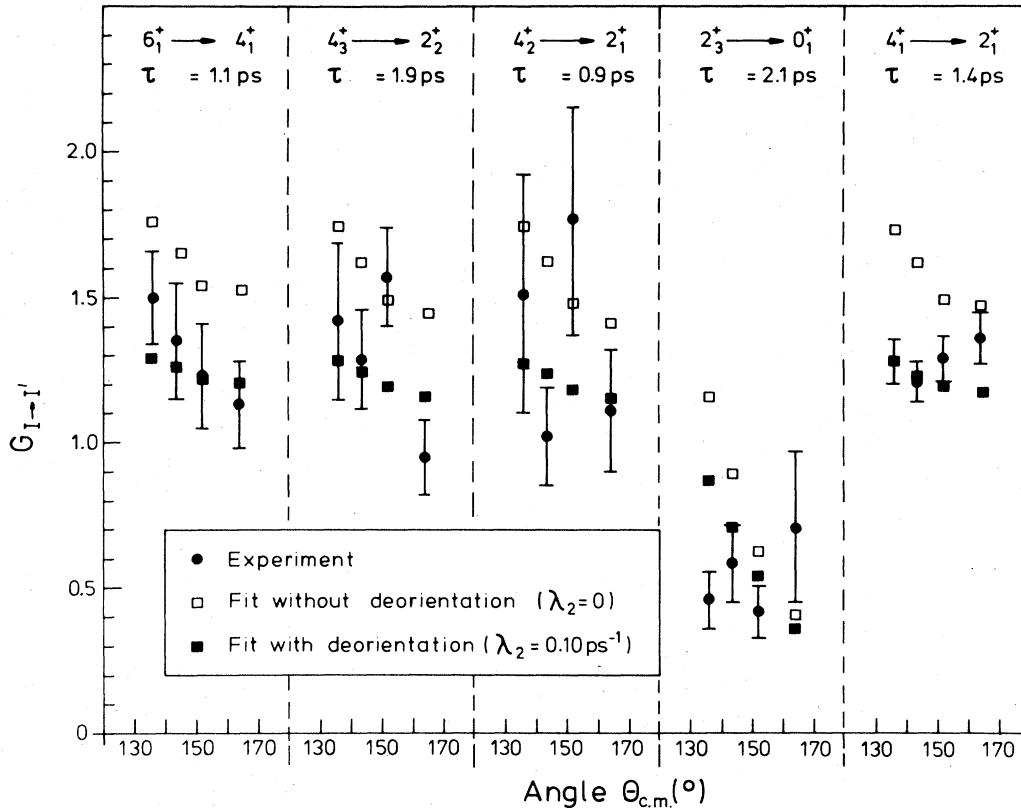


FIG. 5. Results of a fit to the double ratios $G_{I \rightarrow I'}$ for transitions from short-lived states from which the deorientation coefficient λ_2 has been extracted. The open squares correspond to $\lambda_2=0$ (no deorientation) and the closed squares correspond to $\lambda_2=0.1 \text{ ps}^{-1}$ (best fit).

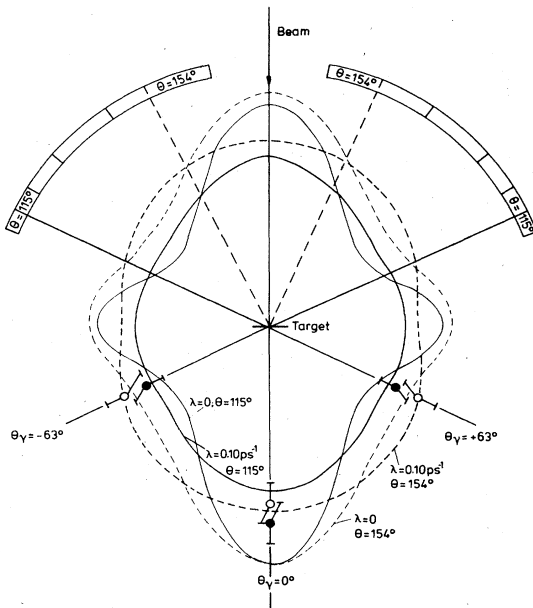


FIG. 6. Gamma ray angular correlation of the $4_1^+ \rightarrow 2_1^+$ transition with deorientation ($\lambda_2=0.1 \text{ ps}^{-1}$) and without deorientation ($\lambda_2=0$). The full lines and dots correspond to the particle angle $\theta=115^\circ$, the dashed lines and circles to $\theta=154^\circ$.

state, we used this attenuation coefficient to calculate those of the other long living nuclear states. An example of such a fit is shown in Fig. 5, whereas Fig. 6 illustrates the dependence of $R_{4 \rightarrow 2}^i(\theta, \theta_\gamma)$ on the γ -ray angle θ_γ at fixed particle angles $\theta^{\text{lab}}=115^\circ$ and 154° . The double ratios $G_{I \rightarrow I'}(\theta)$ do not depend sensitively on the $E2$ matrix elements; we thus used a preliminary set and checked its consistency at the end of the analysis.

D. Details of the fitting procedure

For a given set of matrix elements $\{\mathcal{M}_k\}$, the program calculates the ratio

$$R_i^f(\theta, \theta_\gamma, \{\mathcal{M}_k\}) = Y_{I \rightarrow I'}(\theta, \theta_\gamma) / Y_{\text{norm}}(\theta, \theta_\gamma), \quad (4)$$

where we have explicitly indicated the dependence of R_i^f on the matrix elements to be determined and the index i refers to the transition $I \rightarrow I'$. As the normalizing transition we have chosen the 777 keV $2_1^+ \rightarrow 0_1^+$ transition in all cases. The quantities R^f and R^e are compared in the χ^2 expression

$$\chi^2 = \sum_{i, \theta, \theta_\gamma} [R_i^e(\theta, \theta_\gamma) - R_i^f(\theta, \theta_\gamma, \{\mathcal{M}_k\})]^2 W_i(\theta, \theta_\gamma), \quad (5)$$

where the weights W_i are the squared errors of R_i^e given in Table I.

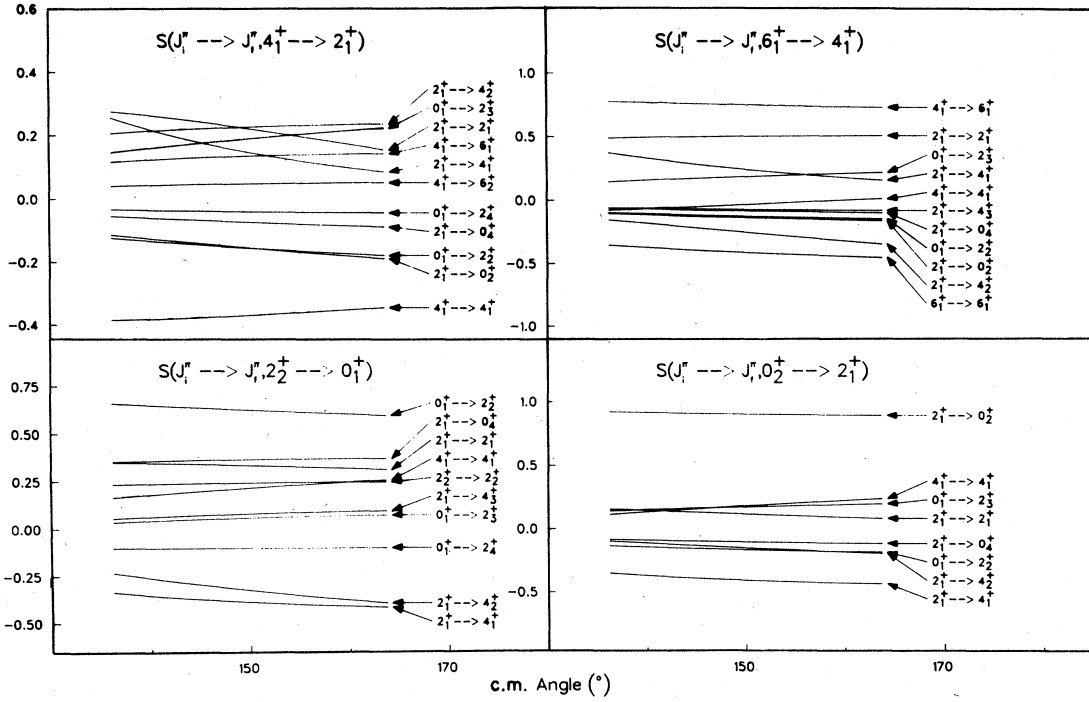


FIG. 7. Partial sensitivity matrix defined in Eq. (8) of the $4_1^+ \rightarrow 2_1^+$, $2_2^+ \rightarrow 0_1^+$, $6_1^+ \rightarrow 4_1^+$, and $0_2^+ \rightarrow 2_1^+$ transitions as a function of the center-of-mass particle angle θ .

To perform the χ^2 minimization we used the linear ansatz

$$R_i^{f(\text{new})}(\theta, \theta_\gamma, \{\mathcal{M}_k\} + \delta\mathcal{M}_k) = R_i^{f(\text{old})}(\theta, \theta_\gamma, \{\mathcal{M}_k\}) + \sum_I A_{ii}(\theta, \theta_\gamma, \{\mathcal{M}_I\}) \delta\mathcal{M}_I, \quad (6)$$

where the partial derivatives A_{ii} are numerically calculated as

$$A_{ii} = [R_i^f(\theta, \theta_\gamma, \{\mathcal{M}_I + \Delta\mathcal{M}_I\}) - R_i^f(\theta, \theta_\gamma, \{\mathcal{M}_I\})] / \Delta\mathcal{M}_I \quad (7)$$

and the $\Delta\mathcal{M}_I$ are the parameter ranges in which the linear ansatz is expected to be valid. The system of linear equations for the unknown $\delta\mathcal{M}_k$ [obtained by setting $d\chi^2/d(\delta\mathcal{M}_I) = 0$] is then solved and the procedure is repeated, as explained above, until the set of matrix elements remains stationary. At the end of each iteration step it was checked that $|\delta\mathcal{M}_k| < |\Delta\mathcal{M}_k|$ for every k otherwise a new set A_{ii} was calculated. As it turns out, a more useful quantity to be studied (and closely related to A_{ki}) is the so-called "sensitivity matrix" defined as¹²

$$S_{J \rightarrow J', I \rightarrow I'}(\theta) = \frac{\Delta R_{I \rightarrow I'}^f(\theta)(\mathcal{M}_k^2)}{R_{I \rightarrow I'}^f(\theta)(\mathcal{M}_k^2)}, \quad (8)$$

where $\Delta R_{I \rightarrow I'}^f(\theta)$ is the difference between two yield ratios for the transition $I \rightarrow I'$ at the particle angle θ corre-

sponding to the reduced $E2$ matrix elements \mathcal{M}_k and $\mathcal{M}_k + \Delta\mathcal{M}_k$. A few elements of the sensitivity matrix are shown in Fig. 7. This figure clearly reveals the complexity of the minimization problem, since over the whole range of θ values many different matrix elements contribute significantly to the relative variation of a given yield.

Another important point in this procedure was the choice of convenient starting values for the $\{\mathcal{M}_k\}$. We were guided to some extent by the approximate knowledge of the absolute values of some $E2$ matrix elements (deduced from level lifetimes). However, as already stressed in earlier works,^{12,13} the sign of the matrix elements is also of importance in the MCE. For the initial choice of these phases as well as for several matrix elements for which no information was available (like quadrupole moments) we relied on the predictions of the IBA-2.⁹

IV. EXPERIMENTAL RESULTS

As a result of the overall minimization procedure, fits to the experimental yield ratios as functions of the scattering angle θ were obtained, which are shown in Fig. 8. Table II lists the experimental and fitted integral yield ratios. The deduced matrix elements (ME) are given in Table IV.

One may note the rather large uncertainties of these matrix elements. Indeed the errors of the final set of parameters cannot be simply obtained in the standard way by the inversion of the normal matrix, but must include several sources of uncertainties. Firstly, the statistical er-

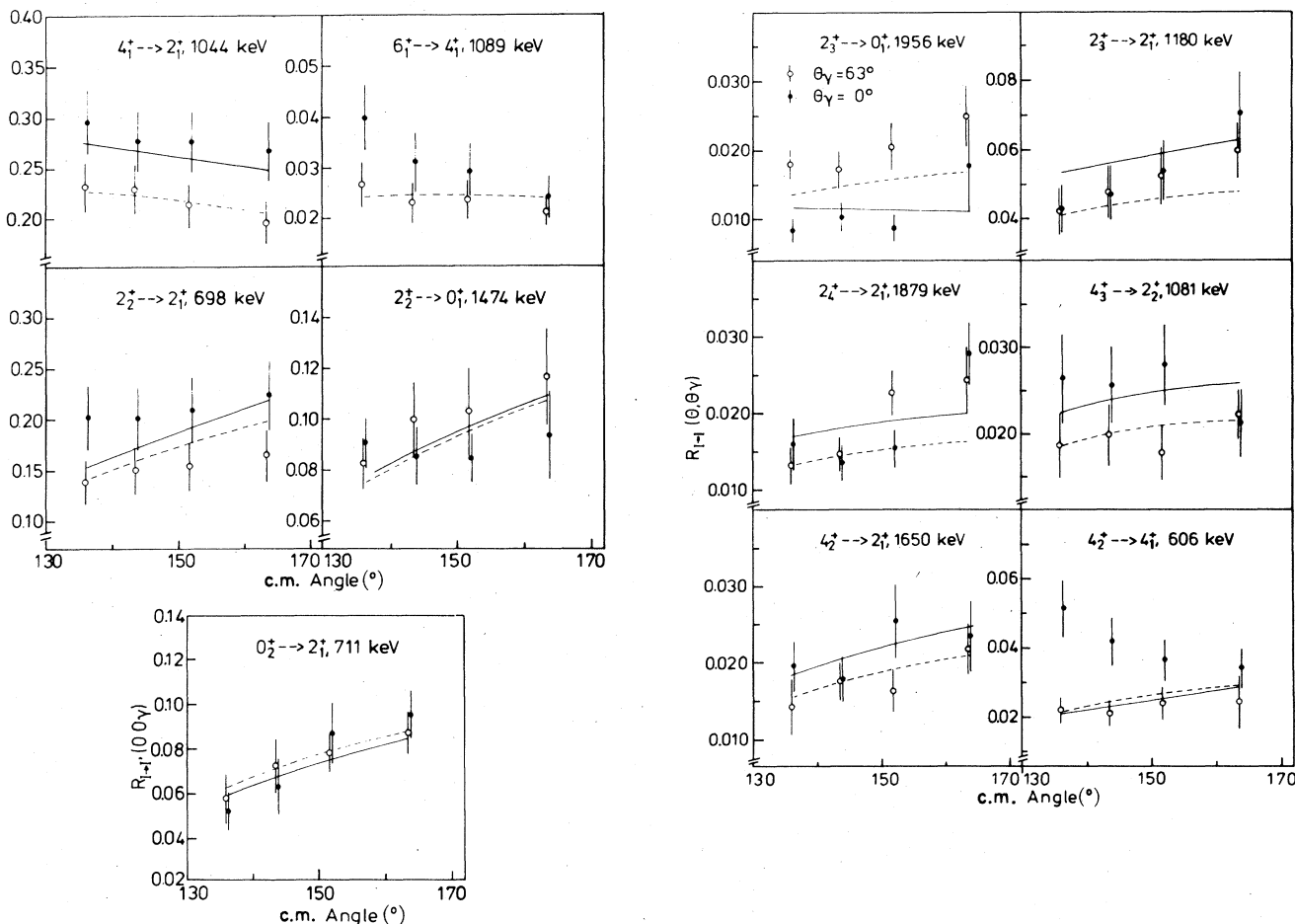


FIG. 8. Fits to the intensity ratios $R_{I \rightarrow I'}(\theta, \theta_\gamma)$ for the transitions indicated. Dots and full lines denote the experimental points respective fit at $\theta_\gamma = 0^\circ$; circles and dashed lines for $\theta_\gamma = 63^\circ$.

rors given include the statistical errors of the data points as well as the uncertainty resulting of the $2_1^+ \rightarrow 0_1^+$ normalizing matrix element of the 777 keV transition. This total statistical error is typically 5–15%. An even larger systematic error which has been added linearly comes, however, from the unknown relative phases of the matrix elements. This error has to be taken into account whenever a certain level can be excited by more than one excitation path. In a transitional nucleus like ^{82}Kr with collective and single-particle degrees of freedom coupled to each other (see below), the situation is less favorable than in a good rotational or vibrational nucleus where only the ground and gamma band plays a role and the phases are fixed with respect to each other. In the present analysis, 7 out of 11 levels observed are fed by more than one excitation path. The variation of the relative phases is usually done by considering the sign of the interference loop

$$P_3(I) = \text{sgn}(\mathcal{M}_{I' \rightarrow I''} \mathcal{M}_{I'' \rightarrow I} \mathcal{M}_{I \rightarrow I'}),$$

where the excitation path $I' \rightarrow I'' \rightarrow I$ interferes with the direct excitation $I' \rightarrow I$. As a starting point, we choose the phases given by the IBA-2 parametrization.⁹ We then first changed $P_3(2_2^+)$; on the basis of the resulting χ^2 ,

$P_3(2_2^+)$ turned out to be positive. Previous determinations of this quantity had resulted in $P_3(2_2^+) < 0$ in ^{194}Pt and ^{102}Ru (Refs. 19 and 20) and $P_2(2_2^+) > 0$ in ^{104}Ru (Refs. 12 and 13). In the next step, $P_3(2_3^+)$ was varied, but no significant difference in χ^2 was observed; likewise, the data did not allow us to fix $P_3(0_3^+)$ nor $P_3(0_4^+)$. The signs of the static quadrupole moments of the 2_1^+ and 4_1^+ states of the ground band turned out to be negative, although the exact values could not be determined, due to the uncertainties of the other matrix elements. The quadrupole moment of the 2_2^+ state was assumed to have an opposite sign as the 2_1^+ state, as predicted by any collective model for the ground and gamma band.

Also given in Table IV are the $B(E2)$ values of the $4_1^+ \rightarrow 2_1^+$ and $6_1^+ \rightarrow 4_1^+$ yrast transitions deduced from previous lifetime measurements.^{7,8} While the result of the $^{70}\text{Se}(\alpha, 2n)$ plunger experiment⁷ for $B(E2, 4^+ \rightarrow 2^+)$ is in agreement with the present study, the values of $B(E2, 6^+ \rightarrow 4^+)$ determined in both plunger experiments^{7,8} do not agree with the present measurement. This is probably a consequence of the very long lifetime of the 8_1^+ yrast state [$\tau = 124(12)$ ps] which dominates the decay function of the $6_1^+ \rightarrow 4_1^+$ transition. The lifetime of the 2920 keV 6_1^+ state obtained from the present Coulomb excitation

TABLE IV. Deduced $E2$ matrix elements \mathcal{M} and $B(E2)$ values. The relative statistical and systematic errors $|\Delta\mathcal{M}/\mathcal{M}|_{\text{stat}}$ and $|\Delta\mathcal{M}/\mathcal{M}|_{\text{sys}}$ are also given. The last column summarizes the previously measured $B(E2)$ values (Refs. 7 and 8).

| E_x (keV) | I^π | E_γ (keV) | \mathcal{M} (e b) | \mathcal{M} | | $B(E2)$ ($e^2\text{fm}^4$) | |
|----------------|---------|---------------------|----------------------------|---|--|------------------------------|---|
| | | | | $ \frac{\Delta\mathcal{M}}{\mathcal{M}} _{\text{stat}}$ | $ \frac{\Delta\mathcal{M}}{\mathcal{M}} _{\text{sys}}$ | present | previous |
| 3167 | 6_2^+ | 1347 | $0.45^{+0.12}_{-0.14}$ | $\frac{+9}{-13}$ | 17 | 156^{+94}_{-82} | $168(46)^a$ |
| 2920 | 6_1^+ | 1099 | $0.74^{+0.17}_{-0.23}$ | $\frac{+8}{-16}$ | 15 | 421(220) | $128^{+52}_{-43}{}^a$ $85^{+43}_{-34}{}^b$ |
| 2656 | 2_4^+ | 1168 | -0.302(54) | 8 | 10 | 182(65) | |
| | | 1181 | 0.462(83) | | | 427(153) | |
| | | 1879 | 0.233(42) | | | 109(39) | |
| | | 2656 | -0.056(10) | | | 6.3(22) | |
| 2556 | 4_3^+ | 736 | 0.368(51) | 8 | 6 | 150(42) | |
| | | 1180 | 0.416(58) | | | 192(54) | |
| | | 1780 | -0.053(7) | | | 3.1(8) | |
| 2450 | 0_4^+ | 975 | 0.46(29) | 36 | 27 | 2110^{+3510}_{-1830} | |
| | | 1673 | 0.11(7) | | | 121^{+203}_{-105} | |
| 2427 | 4_2^+ | 606 | 0.87(11) | 6 | 6 | 840(210) | |
| | | 952 | 0.41(5) | | | 187(46) | |
| | | 1650 | 0.15(2) | | | 25(7) | |
| 2172 | 0_3^+ | 697 | 0.15(7) | 4 | 45 | 225^{+258}_{-161} | |
| | | 1395 | -0.067(33) | | | 45^{+55}_{-33} | |
| 1957 | 2_3^+ | 1180 | 0.272(79) | 6 | 23 | 148^{+98}_{-74} | |
| | | 1957 | 0.061(18) | | | $7.4^{+5.1}_{-3.7}$ | |
| 1821 | 4_1^+ | 1044 | $0.78^{+0.13}_{-0.16}$ | $\frac{+5}{-8}$ | 11 | 676^{+230}_{-270} | $470^{+470}_{-235}{}^a$ |
| 1487 | 0_2^+ | 711 | 0.18(3) | 5 | 11 | 324(108) | |
| 1475 | 2_2^+ | 698 | $-0.28^{+0.09}_{-0.06}$ | $\frac{+11}{-8}$ | $\frac{+20}{-14}$ | 155^{+96}_{-68} | |
| | | 1475 | $-0.035^{+0.011}_{-0.008}$ | | | $2.5^{+1.5}_{-1.1}$ | |
| 777 | 2_1^+ | 777 | $0.474(10)^c$ | | | | 450(21) ^c |

^aReference 7.

^bReference 8.

^cReference matrix element, Ref. 5.

study, $\tau = 1.2^{+1.4}_{-0.4}$ ps, thus needs further confirmation.

We finally mention a difficulty which arose in the analysis of the decays of the 2656 keV 2_4^+ and 1488 keV 0_2^+ states. The 2656 keV level has been observed in the β decays of $^{82}\text{Br}^m$ and $^{82}\text{Rb}^g$ and gamma ray branching ratios of this state have been derived in both decays.⁶ In the $^{82}\text{Rb}^g$ decay, a 8(4)% branch of the 1168 keV $2_4^+ \rightarrow 0_2^+$ and a 59(4)% branch for the 1879 keV $2_4^+ \rightarrow 2_1^+$ transition have been reported. These numbers are, however, at variance with the branching ratios of 33(3)% and 37(2)% for the same transitions obtained in the β decay of $^{82}\text{Br}^m$ (Ref. 6). This discrepancy naturally affects the $E2$ strengths in the excitation of the 2656 keV 2_4^+ state itself, but also the $0_2^+ \rightarrow 2_1^+$ $E2$ matrix element which decreases substantially in the fit, if the observed intensity of the 711 keV $0_2^+ \rightarrow 2_1^+$ line is merely due to the cascade decay of the 2656 keV state rather than to the Coulomb excitation of the 1488 keV 0_2^+ state itself. The upper limit of <18% of the 1168 keV $2_4^+ \rightarrow 0_2^+$ branching ratio deduced from the present data motivates us to adopt the reported branching ratios of the $^{82}\text{Rb}^g$ decay in our analysis.

V. NUCLEAR MODEL INTERPRETATIONS

The nucleus ^{82}Kr lies about halfway between the $N=50$ shell closure and the domain of large quadrupole

deformation ($\beta=0.38$) in $^{74,76}\text{Kr}$. Indeed, several collective models have been applied in the past which describe the shape transition in these neutron deficient Kr isotopes (Refs. 9–11 and 21). The moderate quadrupole deformation in ^{82}Kr of $\beta=0.18$ deduced from $B(E2, 2_1^+ \rightarrow 0_1^+) = 450(21) e^2\text{fm}^4$ (Ref. 5) makes it a candidate for a transitional nucleus with possibly vibrational-like structure. As strong backbendings occur near the 8^+ yrast and yrare states which have been associated with $g_{9/2}$ neutron and proton ($2qp$) alignment,^{7,8} we restrict the discussion to the states up to spin $I=6$ and 2.9 MeV excitation energy for which the present experiment, together with the previously measured branching and $E2/M1$ mixing ratios,^{6,7,22} has provided some 20 quadrupole transition probabilities (see Table IV).

A. Model parameters

The models considered are the Davydov triaxial rotor,²¹ the collective model by Gneuss and Greiner,¹¹ the interacting boson model⁹ with proton and neutron bosons (IBA-2), and the nuclear field theory (NFT).¹ Without giving a detailed description of these models, we shortly recapitulate their essential parameters and then compare the predicted band structures with the observed ones. Numerical results are given in Table V.

TABLE V. Comparison of the experimental $B(E2)$ values with the model predictions discussed in the text.

| State E_x (keV) | Transition E_γ (keV) | I_i^π | I_f^π | Expt. | $B(E2)$ ($e^2\text{fm}^4$) | | | |
|-------------------------|-----------------------------------|-----------|-----------|------------------------|------------------------------|-------|-----|-----|
| | | | | | AR | IBA-2 | CM | NFT |
| 3167 | 1347 | 6_2^+ | 6_1^+ | 156^{+94}_{-82} | | | | |
| 2920 | 1099 | 6_1^+ | 4_1^+ | 421(220) | 779 | 739 | 780 | 671 |
| 2656 | 1181 | 2_4^+ | 2_2^+ | 427(153) | | 147 | | |
| | 1879 | | 2_1^+ | 109(39) | | 4.5 | | |
| | 2656 | | 0_1^+ | 6.3(22) | | 0.3 | | |
| 2556 | 736 | 4_3^+ | 4_1^+ | 150(42) | 121 | 275 | | |
| | 1180 | | 2_2^+ | 192(54) | 216 | 360 | 372 | 270 |
| | 1779 | | 2_1^+ | 3.1(8) | 9 | 2.4 | 22 | 48 |
| 2450 | 975 | 0_4^+ | 2_2^+ | 2110^{+3510}_{-1830} | | 325 | | |
| | 1674 | | 2_1^+ | 121^{+203}_{-105} | | 10.5 | | |
| 2427 | 952 | 4_2^+ | 2_2^+ | 187(46) | 216 | 360 | 372 | 270 |
| | 1650 | | 2_1^+ | 25(7) | 9 | 2.4 | 22 | 48 |
| 2172 | 697 | 0_3^+ | 2_2^+ | 225^{+258}_{-161} | | 338 | | 338 |
| | 1395 | | 2_1^+ | 45^{+55}_{-33} | | 338 | | 169 |
| 1957 | 1180 | 2_3^+ | 2_1^+ | 148^{+98}_{-74} | | 169 | | |
| | 1957 | | 0_1^+ | $7.4^{+5.1}_{-3.7}$ | | 8.4 | | |
| 1821 | 1044 | 4_1^+ | 2_1^+ | 676^{+230}_{-270} | 621 | 678 | 678 | 617 |
| 1475 | 698 | 2_2^+ | 2_1^+ | 155^{+96}_{-68} | 558 | 556 | 590 | 584 |
| | 1475 | | 0_1^+ | $2.5^{+1.5}_{-1.1}$ | 4.5 | 20 | 10 | 8.5 |
| 777 | 777 | 2_1^+ | 0_1^+ | 450(21) ^a | 450 | 450 | 450 | 450 |

The *Davydov triaxial rotor model* (AR) (Ref. 21) assumes rigid rotation of a triaxial spheroid. The level energies and static and transitional $E2$ moments depend on two parameters: the intrinsic quadrupole moment, chosen here as $eQ_0 = 150 e \text{ fm}^2$, deduced from the $2_1^+ \rightarrow 0_1^+$ transition probability, and the triaxiality parameter $\gamma = 27.5^\circ$ obtained from the measured ratio of $B(E2)$ values $B(E2, 2_2^+ \rightarrow 0_1^+)/B(E2, 2_1^+ \rightarrow 0_1^+) = 0.005(3)$.

The *collective model by Gneuss and Greiner* (CM) (Ref. 11) is also restricted to nuclear deformations of quadrupole-type, but can describe any couplings between rotational and vibrational excitation modes. The Hamiltonian is specified by six stiffness and two mass parameters which have to be fitted to the experimental level scheme. In the case of a transitional nucleus of small deformation and/or the occurrence of quasiparticle states, the proper selection of the collective states can be rather difficult. Therefore, the deduced potential energy surface parameters defining the shape(s) of the nucleus depend on the interpretation of the experimental level scheme. The CM potential energy surface of ^{82}Kr proposed by Sedlmayr¹¹ has two pronounced minima, a prolate one at $\beta = 0.20$, $\gamma = 0^\circ$ and a triaxial one at $\beta = 0.35$, $\gamma = -40^\circ$, where the Lund convention of the sign of γ has been adopted.²³ The potential contains large anharmonic terms. The parameters of the Hamiltonian are $B_2 = 19.44 \cdot 10^{-42} \text{ MeV s}^2$, $P_3 = 15.22 \cdot 10^{39} \text{ MeV}^{-1} \text{ s}^{-2}$, $C_2 = 174.14 \text{ MeV}$, $C_3 = 2.04 \cdot 10^4 \text{ MeV}$, $C_4 = -3.81 \cdot 10^4 \text{ MeV}$, $C_5 = -7.29 \cdot 10^5 \text{ MeV}$, $C_6 = 1.61 \cdot 10^6 \text{ MeV}$, and $D_6 = 9.03 \cdot 10^5 \text{ MeV}$. Collective potential energy surfaces in ^{82}Kr have also been calculated with a number of other approaches: Nazarewicz *et al.*²³ applied the Strutinsky-Bogolyubov cranking approach which predicts a rather flat energy surface with a minimum at $\beta = 0.15$, $\gamma \simeq 0^\circ$ (if pairing correlations are being included). Likewise,

Bengtsson *et al.*²⁴ and Bucurescu *et al.*²⁵ obtained flat potential energy landscapes with a minimum near $\beta = 0.10$.

The *interaction boson model* (IBA-2) (Ref. 9) has been successfully applied to the even krypton isotopes by Gelberg and Kaup. More recently, Hellmeister *et al.*^{4,26} have shown that the $B(E2)$ values of the ground, gamma, and octupole bands in $^{76,78,80}\text{Kr}$ are also well reproduced by this model, with very few parameters adjusted individually in each isotope. The IBA-2 Hamiltonian requires the following parameters in the description of the positive-parity bands: the numbers N_π and N_ν of the proton and neutron bosons, the boson energy ϵ , the quadrupole coupling constant κ , χ_π , and χ_ν , the boson exchange term of Majorana-type, and the effective charges q_π and q_ν of the proton respective neutron bosons. In the calculation of the $E2$ transition strengths in ^{82}Kr , we adopted the previously proposed parameters:^{8,9} $N_\pi = 4$, $N_\nu = 2$, $\epsilon = 1.15 \text{ MeV}$, $\kappa = -0.19 \text{ MeV}$, $\chi_\pi = 0.925$, $\chi_\nu = -1.127$, $a = 0.1 \text{ MeV}$, $q_\pi = 8.8 e \text{ fm}^2$, and $q_\nu = 4.4 e \text{ fm}^2$.

The *nuclear field theory* (NFT) (Ref. 10) as an alternative semimicroscopic approach to nuclear collective motion has been applied by Maglione¹⁰ to the low-lying states of the Kr isotopes. The three force parameters of the NFT pairing-plus-quadrupole Hamiltonian are the correlation energy Z_s (Z_d) of a pair interacting by a monopole (quadrupole) pairing interaction which have been chosen as $Z_s = 2.1 \text{ MeV}$, $Z_d = 0.25 \text{ MeV}$, and $\kappa = 1.5 \text{ MeV}$.

B. Comparison of the measured transition strengths with the model predictions

Ground band. While the experimental $B(E2, 4_1^+ \rightarrow 2_1^+)$ is well reproduced in all models considered, it is

noteworthy that the $B(E2, 6_4^+ \rightarrow 4_1^+)$ value falls below the predicted values. This reduction is most likely due to the existence of three closely spaced 6^+ states at 2920, 3167, and 3256 keV which can mix with each other and share in their decay the collective $E2$ strength.^{7,8} Indeed, the summed $E2$ strengths of these three 6^+ states exhausts the rotational value. While the natures of the two lowest 8^+ states at 3462 and 4016 keV as aligned $g_{9/2}$ neutron respective proton ($2qp$) states can be inferred from a recent g -factor measurement of the 8^+ yrast state in the isotope ^{84}Sr ,²⁷ one may consider the partially aligned ($2qp$) states as candidates for the 6_2^+ and 6_3^+ states in ^{82}Kr .

Gamma band. Kemnitz *et al.*⁷ interpreted the 1475 keV 2_2^+ -2094 keV 3^+ -2556 keV 4_3^+ -3186 keV 5^+ sequence as the gamma band. The fact that the 2556 keV state is seen in Coulomb excitation and the $E2$ type of angular correlation of the 1081 keV transition favors the $I^\pi=4^+$ assignment to the 2556 keV level made by these authors over the $I^\pi=3^-$ assignment tentatively made by Meyer *et al.*⁶

In the AR model, the triaxiality parameter γ can be directly deduced from the level energies of the 2_1^+ and 2_2^+ states.²¹ This ratio should be smaller than 0.5, as compared to 0.52 in ^{82}Kr , 0.54 in ^{84}Sr ,²⁸ and 0.53 in ^{86}Zr .²⁹ A ratio larger than 0.50 can be understood if the assumed rigidity of the rotor is relaxed and vibrations are taken into account. As mentioned before the predicted potential energy surfaces (Refs. 11 and 23–25) imply strong anharmonic terms; the IBA-2 representation is close to the SU(5) anharmonic vibrator limit.⁶ Another hint to the softness of ^{82}Kr is the odd-even clustering within the γ band. A rigid triaxial rotor would give rise to a $(2^+, 3^+)$, $(4^+, 5^+)$, . . . clustering, while a γ -unstable potential produces a $(3^+, 4^+)$, $(5^+, 6^+)$, . . . clustering.³⁰ In Fig. 9 the

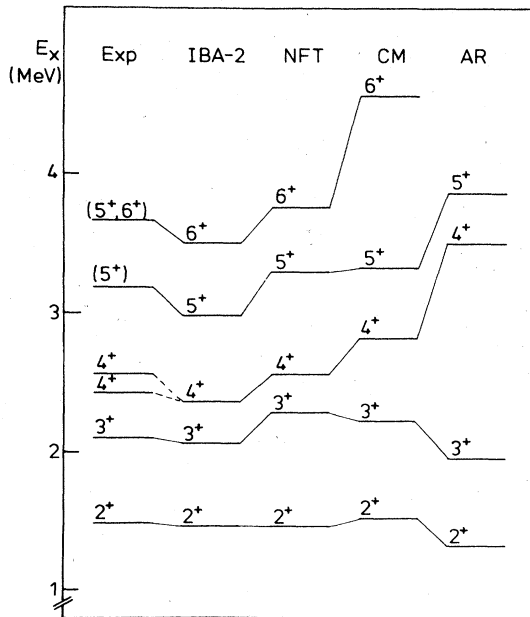


FIG. 9. Comparison of the experimental energies of the gamma band with the model predictions discussed in the text.

experimental level energies of the presumed γ band are compared with the model predictions: the slight $(3^+, 4^+)$ clustering points to a γ -soft nuclear shape.

Let us now discuss in more detail the structures of the two closely spaced 2427 keV 4_2^+ and 2556 keV 4_3^+ states. On the basis of the $E2$ branching ratios to the 2_1^+ and 2_2^+ states, Kemnitz *et al.*⁷ have favored the 4_3^+ state as a member of the gamma band, while they suggested a $(\pi f_{5/2} \pi p_{3/2})$ ($2qp$) configuration for the 4_2^+ level. Looking at the absolute transition strengths determined in the present experiment (see Table V), we find moderately enhanced values of $B(E2, 4^+ \rightarrow 2_2^+) \approx 190 e^2 \text{fm}^4$ and very small values of $B(E2, 4^+ \rightarrow 2_1^+) = 3$ respectively $25 e^2 \text{fm}^4$ in the decay of both 4^+ states. The model predictions are $B(E2, 4_\gamma \rightarrow 2_2^+) = 220-370 e^2 \text{fm}^4$ and $B(E2, 4_\gamma \rightarrow 2_1^+) = 2-50 e^2 \text{fm}^4$. It thus appears to us that the two 4^+ states are again mixed and share the collective $4_\gamma^+ \rightarrow 2_\gamma^+$ $E2$ strength.

The 1488 keV 0_2^+ state. In many nuclei of this mass region, the low excitation energy of the 0_2^+ state has been found difficult to interpret.^{31,32} The IBA-2 and NFT considered here place the first excited collective (two-photon) 0^+ state near 2 MeV and therefore close to the observed 0_3^+ level at 2172 keV, while the CM interprets the 0_2^+ state as the band head of the β band.¹¹ A possible interpretation of this low-lying 0_2^+ state as a pairing vibration (with some admixture of the two-phonon 0^+ state) has been proposed by Takada and Tazaki.³³ These authors predict, however, the pairing vibration in ^{82}Kr at 2170 keV and a reduced monopole strength to the ground state of $\rho(E0, 0_2^+ \rightarrow 0_1^+) = 0.45$. Experimentally, this quantity can be deduced from the ratio

$$B(E0, 0_2^+ \rightarrow 0_1^+) / B(E2, 0_2^+ \rightarrow 2_1^+) = 0.0181(21)$$

measured by Zemel *et al.*³⁴ and the value

$$B(E2, 0_2^+ \rightarrow 2_1^+) = 324(108) e^2 \text{fm}^4$$

measured in the present study. The deduced value $\rho(0_2^+ \rightarrow 0_1^+) = 0.089(15)$ disagrees, however, with the above prediction, but it also disagrees with the vibrational value

$$\rho(0_2^+ \rightarrow 0_1^+) = 3 \left(\frac{2}{5}\right)^{1/2} Z\beta^2 / 4\pi = 0.176.$$

The interpretation of the 0_2^+ state thus remains unclear.

The 1957 keV 2_3^+ state. According to the IBA-2 classification of the ^{82}Kr levels proposed by Meyer *et al.*,⁶ this state has been interpreted as the lowest number of those bands which do not have maximum F spin $F_{\text{max}} = (N_\pi + N_\nu) / 2 = 3$.⁹ Recently, Hamilton *et al.*³⁵ and Otsuka and Ginocchio³⁶ pointed out that the energy and $E2$ decays of this 2^+ state determine the force constant a of the boson exchange term in the Hamiltonian and the ratio of neutron and proton effective charges q_π / q_ν . In the present Coulomb excitation experiment, the two decay branches of the 1957 keV state have been observed (the 1180 and 1957 keV lines in Fig. 4) with transition probabilities

$$B(E2, 2_3^+ \rightarrow 2_1^+) = 148 e^2 \text{fm}^4$$

and

$$B(E2, 2_3^+ \rightarrow 0_1^+) = 7.4 e^2 \text{fm}^4.$$

For the ratio $q_\pi/q_\nu=2$ adopted in this nucleus, the respective IBA-2 predictions are 169 and $8.4 e^2 \text{fm}^4$ in excellent agreement with the experiment. Assuming, however, equal effective charges $q_\pi/q_\nu=1$, one would obtain 145 and $0.3 e^2 \text{fm}^4$, where the latter value is in severe disagreement with the data.

On the basis of the measured energy and $E2$ decay probabilities, we thus conclude that the 1957 keV 2^+ state has indeed lower F spin $F=F_{\text{max}}-1=2$. This interpretation is further supported by the existence of a 1^+ level at 2480 keV which usually is taken as a fingerprint of this class of states.³⁷ Furthermore, as already suggested in an earlier paper,⁵ the variation of the ratio q_π/q_ν along the Kr isotope chain has been established. We remind that equal boson charges $q_\pi=q_\nu$ are required to fit the $E2$ transition strengths in the strongly deformed ^{78}Kr nucleus.⁴ The ratio $q_\pi/q_\nu=2$ found in ^{82}Kr is close to 2.2 recently proposed for the vibrational nucleus ^{148}Sm .³⁶

The states at 2172 keV (0_3^+), 2450 keV (0_4^+), and 2656 keV (2_4^+). According to their excitation energies, these levels have been tentatively attributed, within the IBA-2 and the anharmonic vibrational models, to excited bands. As mentioned before, the 2172 keV 0_3^+ state appears as a member of the two-phonon triplet. The 2450 keV 0_4^+ and 2656 keV 2_4^+ levels may therefore be members of the three-phonon multiplet. This interpretation implies that the selection rules for $E2$ transitions within the multiphonon configurations should govern the decay modes of these states, e.g., the forbidden $2_4^+ \rightarrow 0_1^+$ and $2_4^+ \rightarrow 2_1^+$ transitions should be very weak ($\Delta n > 1$), while the allowed $\Delta n = 1$ $0_3^+ \rightarrow 2_1^+$, $0_4^+ \rightarrow 2_2^+$, and $2_4^+ \rightarrow 2_2^+$ $E2$ transitions should have normal collective strengths. Looking at Table V, we note that, within their fairly large uncertainties, the experimental $B(E2)$ values follow this trend.

VI. CONCLUSIONS

We have demonstrated in this study that the multiple Coulomb excitation process can be successfully applied to a relatively light nucleus ($Z=36$) of moderate quadrupole deformation ($\beta=0.18$). States up to $I^\pi=6^+$ and 3 MeV excitation energy have been observed in the $^{82}\text{Kr}+^{208}\text{Pb}$ collisions. Although in the population of high spin states in this mass region, Coulomb excitation cannot compete with heavy ion fusion evaporation reactions, the excitation of many states with spins up to $I=6$ has been essential in clarifying the structure of this transitional nucleus. On the other hand, one should also note that the highly correlated level scheme in a narrow spin window made the analysis of the measured gamma ray yields very tedious

and introduced fairly large uncertainties in the resulting $B(E2)$ values.

From the present and previous investigations, ^{82}Kr is found to have a complicated structure which clearly exhibits collective and single-particle degrees of freedom. While the 2^+ and 4^+ levels of the ground band are collective, aligned ($2qp$) configurations mix with the collective 6_1^+ state and dominate the yrast spectrum for $I > 8$. A similar behavior seems to be present in the γ band, especially for the strongly mixed 4_2^+ and 4_3^+ states. It thus appears that these ($2qp$) components should be explicitly taken into account for the states above 2 MeV excitation. On the other hand, it is the occurrence of these noncollective components, together with the limited precision of the deduced transition moments, which prevents a more rigorous test of the collective models discussed before.

While Meyer *et al.*⁶ have shown that the observed level structure below 3 MeV lines up with an IBA-2 fit adjusted to few low-lying states, the measured $E2$ transitional moments provide additional support for this interpretation (although difficulties remain in the interpretation of $E2$ decays of the 2_2^+ and 0_2^+ states). One of the essential results of the present study are the $E2$ transition strengths of the multiphonon 0_3^+ , 0_4^+ , 2_3^+ , and 2_4^+ states. In particular, the excitation energy and $E2$ decay strengths of the 1957 keV 2_3^+ state are in excellent agreement with the predictions of the IBA-2 model and give conclusive evidence for this state having lower F spin $F=F_{\text{max}}-1=2$. All other states observed seem to have maximum F spin $F=F_{\text{max}}=3$ and therefore fully symmetric wave functions concerning proton and neutron bosons. The properties of this 2_3^+ state corroborate the IBA-2 parameters chosen previously⁹ and fix the ratio $q_\pi/q_\nu=2$ of the proton and neutron charges.⁵ An additional proof for the $F_{\text{max}}-1$ character of this state and the 2480 keV 1^+ state would be a measurement of the $2_3^+ \rightarrow 2_1^+$ and $1^+ \rightarrow 0_1^+$ $M1$ transition moments which are expected to be comparable to the single-particle unit.³⁷

ACKNOWLEDGMENTS

The authors are indebted to H. Stelzer for his help in constructing and testing the charged particle detector, and to H. Folger for the preparation of the targets. We appreciate with thanks the help of H.-J. Wollersheim and H. Grein during the data taking as well as discussing with A. Gelberg, F. Iachello, T. Otsuka, and D. Schwalm. We also acknowledge the permission to quote unpublished results of E. Maglione. The calculations were performed at the Gesellschaft für Wissenschaftliche Datenverarbeitung, Göttingen. This work was supported by Deutsches Bundesministerium für Forschung und Technologie.

*Present address: State University of New York, Stony Brook, NY 11794.

¹E. Nolte, Y. Shida, W. Kutschera, T. Prestele, and H. Morinaga, *Z. Phys.* **268**, 267 (1974).

²L. Funke, J. Döring, F. Dubbers, P. Kemnitz, E. Will, G. Winter, V. G. Kiptilij, M. F. Kudojarov, I. Kh. Lemberg, A.

A. Pasternak, A. S. Mishin, L. Hildingsson, A. Johnson, and Th. Lindblad, *Nucl. Phys.* **A355**, 228 (1981).

³R. B. Piercy *et al.*, *Phys. Rev. Lett.* **47**, 1514 (1981).

⁴H. P. Hellmeister, J. Keinonen, K. P. Lieb, U. Kaup, R. Rascher, R. Ballini, J. Delaunay, and H. Dumont, *Nucl. Phys.* **A332**, 241 (1979); *Phys. Lett.* **85B**, 34 (1979).

- ⁵J. Keinonen, K. P. Lieb, H. P. Hellmeister, A. Bockisch, and H. Emling, Nucl. Phys. **A376**, 246 (1982).
- ⁶R. A. Meyer, J. F. Wild, K. Eskola, M. E. Lieno, S. Väisälä, K. Forssten, U. Kaup, and A. Gelberg, Phys. Rev. C **27**, 2217 (1983).
- ⁷P. Kemnitz, P. Ojeda, J. Döring, L. Funke, L. K. Kostov, H. Rotter, E. Will, and G. Winter, Nucl. Phys. **A425**, 493 (1984).
- ⁸S. Brüssermann, J. Keinonen, H. P. Hellmeister, and K. P. Lieb, Z. Phys. A **304**, 335 (1982).
- ⁹T. Otsuka, A. Arima, F. Iachello, and I. Talmi, Phys. Lett. **76B**, 139 (1978); U. Kaup and A. Gelberg, Z. Phys. A **293**, 311 (1979).
- ¹⁰R. Broglia, K. Marsuyangi, H. Sofia, and A. Vitturi, Nucl. Phys. **A348**, 237 (1980); E. Maglione, private communication.
- ¹¹G. Gneuss and W. Greiner, Nucl. Phys. **A171**, 449 (1971); M. Sedlmayer, doctoral thesis, Universität Frankfurt, 1976 (unpublished).
- ¹²J. Stachel, N. Kaffrell, E. Grosse, H. Emling, H. Folger, P. Kulessa, and D. Schwalm, Nucl. Phys. **A383**, 429 (1982).
- ¹³J. Stachel, P. Hill, N. Kaffrell, H. Emling, H. Grein, E. Grosse, Ch. Michel, H. J. Wollersheim, D. Schwalm, S. Brüssermann, and F. R. May, Nucl. Phys. **A419**, 589 (1984).
- ¹⁴H. Stelzer, in *Lecture Notes in Physics*, edited by W. von Oertzen (Springer, Berlin, 1983), Vol. 178, p. 25.
- ¹⁵G. Gaukler, H. Schmidt-Böcking, R. Schuch, R. Schule, H. J. Specht, and I. Tserruya, Nucl. Instrum. Methods **141**, 115 (1977).
- ¹⁶K. Adler and A. Winther, *Electromagnetic Excitation* (North-Holland, Amsterdam, 1975).
- ¹⁷K. P. Lieb, A. M. Nathan, and J. W. Olness, Hyp. Int. **5**, 113 (1978).
- ¹⁸A. Abragam and R. V. Pound, Phys. Rev. **92**, 943 (1953).
- ¹⁹L. Hasselgren, C. Fahlander, J. E. Thun, A. Bockisch, and F. J. Bergmeister, Phys. Lett. **83B**, 169 (1979).
- ²⁰C. Fahlander, L. Hasselgren, J. E. Thun, A. Bockisch, A. M. Kleinfeld, A. Gelberg, and K. P. Lieb, Phys. Lett. **60B**, 347 (1976).
- ²¹A. S. Davydov and G. T. Filippov, Nucl. Phys. **8**, 237 (1958); A. S. Davydov, *ibid.* **24**, 82 (1961).
- ²²P.-T. Callaghan, N. J. Stone, and R. B. Alexander, Hyp. Int. **3**, 267 (1977).
- ²³W. Nazarewicz, J. Dudek, R. Bengtsson, T. Bengtsson, and I. Ragnarsson, Nucl. Phys. **A435**, 397 (1985); W. Nazarewicz, private communication.
- ²⁴R. Bengtsson, P. Möller, J. R. Nix, and Jing-ye Zhang, Phys. Scr. **29**, 402 (1984).
- ²⁵D. Bucurescu, G. Constantinescu, D. Cutoiu, M. Ivascu, and N. V. Zamfir, J. Phys. G **7**, L123 (1981).
- ²⁶H. P. Hellmeister, K. P. Lieb, and J. Panqueva, in *Interacting Bose-Fermi Systems in Nuclei*, edited by F. Iachello (Plenum, New York, 1981), p. 65; K. P. Lieb, J. Panqueva, H. P. Hellmeister, and T. Otsuka, *Proceedings of the XXth Winter Meeting on Nuclear Physics, Bormio*, edited by I. Iori (Ric. Scient. Educaz. Permanente, Milano, 1982), p. 76.
- ²⁷C. Broude, E. Dafni, A. Gelberg, M. B. Goldberg, G. Goldring, M. Hass, O. C. Kistner, and A. Zemel, Phys. Lett. **105B**, 119 (1981).
- ²⁸A. Dewald, U. Kaup, W. Gast, A. Gelberg, H. W. Schuh, K. O. Zell, and P. von Brentano, Phys. Rev. C **25**, 226 (1982).
- ²⁹J. Hattula, S. Justinen, H. Helppi, A. Pakkanen, M. Piiparinen, S. Elfström, and Th. Lindblad, Phys. Rev. C **28**, 1860 (1983).
- ³⁰L. Willets and M. Jean, Phys. Rev. **102**, 788 (1956).
- ³¹K. J. Weeks, T. Tamura, T. Udagawa, and F. J. W. Hahne, Phys. Rev. C **24**, 703 (1981); M. Kregar and M. V. Mihailovic, Nucl. Phys. **93**, 402 (1967).
- ³²K. Kumar, J. Phys. G **4**, 849 (1978).
- ³³K. Takada and S. Tazaki, Nucl. Phys. **A395**, 165 (1983).
- ³⁴A. Zemel, T. Hageman, J. J. Hamill, and J. van Klinken, Phys. Rev. C **31**, 1483 (1985).
- ³⁵W. D. Hamilton, A. Irbäck, and J. P. Elliott, Phys. Rev. Lett. **53**, 2469 (1984).
- ³⁶T. Otsuka and J. N. Ginocchio, Phys. Rev. Lett. **54**, 777 (1985).
- ³⁷D. Bohle, A. Richter, W. Steffen, A. E. L. Dieperink, N. Lo Iudice, F. Palumbo, and O. Scholten, Phys. Lett. **137B**, 27 (1984); A. E. L. Dieperink, Comments Nucl. Part. Phys. **14**, 25 (1984).